Available online at www.sciencedirect.com
SCIENCE DIRECT®
Composites Science and Technology 65 (2005) 1306–1320
COMPOSITES SCIENCE AND TECHNOLOGY
www.elsevier.com/locate/compscitech

Three-dimensional features of void morphology in resin transfer molded composites

Youssef K. Hamidi, Levent Aktas, M. Cengiz Altan *

School of Aerospace and Mechanical Engineering, University Of Oklahoma, Norman, OK 73019, USA

Received 9 November 2004; accepted 13 January 2005
Available online 11 February 2005

Abstract

Detailed analyses of shape, size, and spatial variations of void morphology are presented for a disk-shaped, resin transfer molded (RTM), E-glass/epoxy composite. The disk is molded at constant injection rate and contains 17.5% E-glass random fiber mats. Voids throughout the composite are evaluated by microscopic image analysis of through-the-thickness and planar surfaces obtained from adjacent radial samples. The void content of 2.15% is obtained from the analysis of through-the-thickness images and believed to be representative of the actual void content in the studied part. Relatively large cylindrical voids are observed in cigar shapes in the planar surfaces, whereas these voids only appear as small irregular or elliptical voids on through-the-thickness surfaces. Along the radial direction, combined effects of void formation by mechanical entrapment and void mobility are shown to yield a complex radial void distribution. It is shown that fewer voids are trapped mechanically with increasing distance from the inlet and most of the medium and small voids that are mobile migrate towards the exit during resin injection. These findings are believed to be applicable not only to RTM, but generally to liquid composite molding processes with varying fluid front velocities.

Keywords: E. Resin transfer molding (RTM); Three-dimensional voidage

1. Introduction

Resin transfer molding (RTM) and other liquid composite molding (LCM) processes are being used in manufacturing near-net-shape, geometrically complex composite parts. In addition to the process versatility and wide range of possible molding materials, attractive features of these processes are lower operational costs and higher production rates compared to alternative manufacturing processes [1]. RTM consists of placing a dry fibrous preform composed of multiple layers into a mold cavity. Subsequently, a thermosetting resin mixed with a curing agent is injected into that mold cavity. During injection, the resin displaces air out of the mold cavity and impregnates the preform before the curing reaction begins. One of the current obstacles to a larger scale application of this process is the formation of defects such as dry spots and voids during resin injection.

Despite several advancements in voidage predictions via modeling and simulations, void formation mechanisms in RTM and similar processes are still not fully understood [2]. This is primarily due to the complexity of the advancing fluid front through intricate preform architectures. Void presence in composites, even in small amounts, is detrimental to their mechanical performance [3–6]. In an earlier article, Judd and Wright [3] reported that regardless of the utilized materials, voids induce reduction in different mechanical properties including interlaminar shear strength (ILSS), tensile and flexural strength and modulus, torsional shear, fatigue resistance, and impact. Ghiorse [4]

* Corresponding author. Tel.: +1 405 325 1737; fax: +1 405 325 1088.
E-mail address: altan@ou.edu (M.C. Altan).

0266-3538/$ - see front matter © 2005 Published by Elsevier Ltd.
doi:10.1016/j.compscitech.2005.01.001

indicated, for carbon/epoxy composites, that each 1% increase in void content induced a 10% reduction in flexural and interlaminar shear strength, and a 5% reduction in flexural modulus. In more recent studies, voidage effects on mechanical properties of RTM composites were investigated. Olivero et al. [5] reported that doubling the void content from 0.35% to 0.72% by volume resulted in a 15% decrease in ultimate tensile strength and 14% decrease in stiffness for RTM composites reinforced with randomly-oriented preforms at 21% fiber volume fraction. Goodwin et al. [6] reported a 7% reduction in ILSS per 1% increase in voidage up to 10% for a RTM composite containing 57% 5-harness satin preform. In addition, the authors observed that failure cracks initiated from medium to large sized voids with sharp corners, but not from small spherical voids. Voidage is also known to affect both the rate and equilibrium level of moisture absorption in composites [7,8]. For instance, Harper et al. [7] reported that an increase from 1% to 5% in void volume fraction induces an increase of around 280% in the initial absorption rate, and 50% in the equilibrium mass gain for an AS4/3502 graphite/epoxy composite.

Controlling void presence in composites involves two different steps: Understanding void formation mechanisms during injection, and developing effective methods for void removal. Although voids can originate from different sources, mechanical air entrapment is believed to be the primary cause of void formation in RTM composites [9–12]. On a macro-scale, the preform is often treated as a porous medium, and the flow is presumed to follow Darcy's law. However, on the micro-scale, i.e. fiber scale, the preform is far from regular and fingering may occur. At the fiber tow level (i.e., scale of the spacing between tows), the flow is driven by viscous forces. In contrast, flow impregnating fiber tows is driven by capillary forces, which at a single fiber scale, becomes dominant over viscous forces. Depending on injection pressure, resin viscosity, fluid front velocity, and other molding parameters, either viscous or capillary flow is likely to lead the other, causing mechanical entrapment of air bubbles. A more detailed analysis of this phenomenon has often been achieved by using the modified capillary number, Ca^*, defined as the non-dimensional ratio of viscous forces to capillary forces [10–13]:

$$Ca^* = \frac{\mu V}{\gamma \cos\theta}, \tag{1}$$

where μ, V, γ, and θ are the impregnating resin viscosity, the macroscopic fluid front velocity, the resin surface tension, and the liquid–fiber contact angle, respectively. At lower Ca^*, capillary flow leads, thus promoting inter-tow void entrapment in the macro-space between fiber tows. At higher Ca^*, on the other hand, viscous flow leads, thus promoting intra-tow void entrapment within fiber tows [10–13].

Patel et al. [12] and Rohatgi et al. [12] measured void contents for various model fluids injected at different velocities during RTM mold filling. All the experimental voidage data are shown to follow a single master curve when plotted as a function of the modified capillary number. This master curve indicated the existence of a preferential range of modified capillary number between 2.5×10^{-3} and 2.5×10^{-2}, within which the void content is minimal (suggesting a micro-equilibrium between viscous and capillary flows). In addition, the authors reported the coexistence of both inter-tow macro-voids and intra-tow micro-voids in this preferential range. For molding processes with $Ca^* < 2.5 \times 10^{-3}$, void content increases exponentially with decreasing Ca^*, and voids encountered are primarily macro-voids. For $Ca^* > 2.5 \times 10^{-2}$, on the other hand, void content increases at a slower rate with increasing Ca^*, and voids observed are dominantly micro-voids.

The definite correlation between modified capillary number and void content confirms that voids originate principally from mechanical entrapment during filling. Based on this finding, a number of authors [14–20] developed theoretical and numerical models, often for simplified architectures, to predict void formation during injection, and consequently propose techniques for void removal. Chan and Morgan [14] developed a one-dimensional model for the impregnation of unidirectional preforms with parallel flow based on Darcy's law. This model predicts a localized void formation at the resin front region but is weakened by the assumption of a simplified fiber arrangement pattern. Patel and Lee [17,18] developed a model for void formation in LCM processes based on the multi-phase Darcy's law. In addition, they offered a criterion based on the local pressure, void size, and contact angle for the movement of trapped voids. More recently, Kang et al. [20] formulated a mathematical model to describe microscopic perturbations in the resin flow front that induce void formation during injection. Once voids are formed, they will be subjected to transport phenomena during filling that alter their spatial distribution and geometrical morphology [17,18,21–23]. For instance, adhesion force between bubbles and fibers originates from the surface tension and the difference between advancing and receding contact angles [22]. In addition, larger voids exhibit larger perimeters and thus have larger adhesion force [22,23].

Several void reduction methods have been presented for RTM composites [10,24–29]. However, determining the best method to reduce voidage involves an in-depth understanding of spatial distribution and detailed morphological characterization of voids throughout the composite. Very few studies explored such detailed void characterization in RTM. In earlier studies, we investi-

gated different aspects of void occurrence and reduction for similar composites [5,29–31]. Through-the-thickness void distribution for the E-glass/epoxy RTM composite disk used in the current study was studied [31]. However, no assessment of voidage was obtained from the planar view, nor was any information obtained on radial variation of void content and morphology.

Microscopic image analysis was chosen not only because it allows the assessment of void location, shape, and size, but also since it has been demonstrated to be among the most accurate methods for measuring void contents [32–35]. However, three-dimensionality of voids is an important aspect of void morphology that is often overlooked in the literature. With all the advantages of microscopic image analysis, one can only assess void morphology two-dimensionally, which does not fully reveal the actual three-dimensional void shapes and sizes. In the current work, we investigate the morphology and spatial distribution of voids based on both planar and through-the-thickness cross-sections. The investigation is performed on two adjacent samples cut along a radial line of the composite. The first sample is analyzed through-the-thickness, while the second is utilized to examine the planar voidage distribution, thus assessing the three-dimensional features of the void morphology. In addition to contrasting the results obtained from both views, more interest is drawn upon radial variation of void content and morphological features of voids to help identify dominant void formation mechanisms.

2. Experimental setup

2.1. Molding procedure

The composite used in this study are fabricated by a custom-made experimental molding setup composed of a hydraulic press; two reservoirs for resin and curing agent; a static mixer; and a center-gated, disk-shaped mold cavity. EPON 815C resin and EPICURE 3282 curing agent (Shell Chemicals) are selected for their low viscosity. Operating the molding press forces the mixture of resin and curing agent into the mold cavity at a constant flow rate of approximately 5.32×10^{-6} m^3/s. Four layers of chopped-strand, E-glass fiber mats having randomly-oriented, planar fibers, and a planar density of 0.4356 kg/m^2 (Fiberglast part #250) are placed in the 3-mm thick mold cavity prior to filling. The details of the molding procedure and experimental setup are described in detail elsewhere [5,29–31]. After injection is complete, the part is cured in the mold for 48 h before demolding, then post-cured at room temperature for two additional weeks to ensure complete cross-linking. The final product is a 3.88-mm-thick resin transfer molded composite disk having 152.4 mm diameter, containing 17.5% fibers by volume.

2.2. Capillary number determination

If the modified capillary number changes spatially, one might expect to see not only spatial variations in void content within a composite part, but also variations in void sizes and shapes. Therefore, determining the range of capillary number involved during an RTM process can be vital to understanding void formation mechanisms, and consequently spatial void distribution and void morphology. The viscosity of the resin-curing agent mixture is measured to be 0.96 N s/m^2 using a Brookfield viscometer (Model DV-II+). In addition, both the surface tension and the advancing contact angle were measured in an earlier study for the same system of resin, curing agent, and random glass-fibers [29]; and their respective values are 36.3×10^{-3} N/m, and 34°. Finally, the fluid front velocity is determined from the injection rate, mold geometry, and fiber content. The modified capillary number can then be obtained by substituting these measured values in Eq. (1). Thus, the modified capillary number is calculated to change along the radial regions between 0.13 and 1.15 (see Table 1).

2.3. Void characterization

Microscopic image analysis of voids is usually conducted on highly localized areas that are assumed to be representative of the whole composite. Then the statistical average of void percentages in the processed images is taken as equivalent to the void volume fraction. This method is so far considered among the most accurate for measuring the true void content [32–35,38]. However, voids can have spatial patterns and non-random distributions due to different molding parameters as was observed in our earlier studies [5,29–31]. These spatial patterns undermine the assumption of random void distribution throughout the composite, thus lowering the accuracy of obtained void contents. In a study on void content measurement in commingled E-glass/polypropylene composites using image analysis, Santulli et al. [38] correlated the error originating from statistical averaging to the number of

Table 1
Modified capillary number variation along the radial flow direction

Radial distance from the injection gate (mm)	7.5	22.5	37.5	52.5	67.5
Modified capillary number (Ca^*)	1.150	0.382	0.229	0.164	0.127

images used. Void content error was observed to steadily decrease with increasing number of images reaching 0.05% only after examining half of the composite surface.

In the current work, instead of statistically averaging randomly selected images, microscopic image analysis is performed over the entire cross-sectional area of the composite using a sufficiently high magnification (i.e., 200×), which enables the identification of voids as small as the radius of a single fiber. Consequently, all identifiable voids at the working magnification throughout the investigated cross-sections are included in the analysis of void content, morphology, and spatial distribution. Due to the planar isotropy of the preform and axisymmetric shape of the mold, the flow is assumed to depend only on the radial location. In order to fully characterize void distribution, two adjacent radial specimens are cut from the fully cured composite disk. Fig. 1 depicts the spatial arrangement of the two investigated samples. The first sample is selected to investigate the planar void distribution, while the second is used for a more traditional through-the-thickness void analysis. As a result of surface machining and subsequent polishing, a total of 0.67-mm-thick layer is removed from the top of the first sample, reserved for planar void analysis. Thereafter, the first 75-mm-long sample is divided into five 15-mm-long regions along the radial direction as shown in Fig. 1(b). A strip width of 2 mm is chosen, as shown in Fig. 1(a), to remain within the axisymmetry of the disk since the inlet has an outer diameter of 6.2 mm. Each $15\text{ mm} \times 2\text{ mm}$ cross-section is then entirely scanned using a MEIJI optical microscope and each void is identified visually. Images of each radial region containing identified voids are then captured using a PC-based CCD camera.

In addition to planar image analysis, void distribution through-the-thickness of the second specimen is also recorded. Hence, five radial regions, with a surface area equivalent to those regions defined for the planar sample, are investigated. As shown in Fig. 1(c), only $8\text{ mm} \times 3.88\text{ mm}$ cross-sections located at the center of corresponding radial regions are investigated. Voids

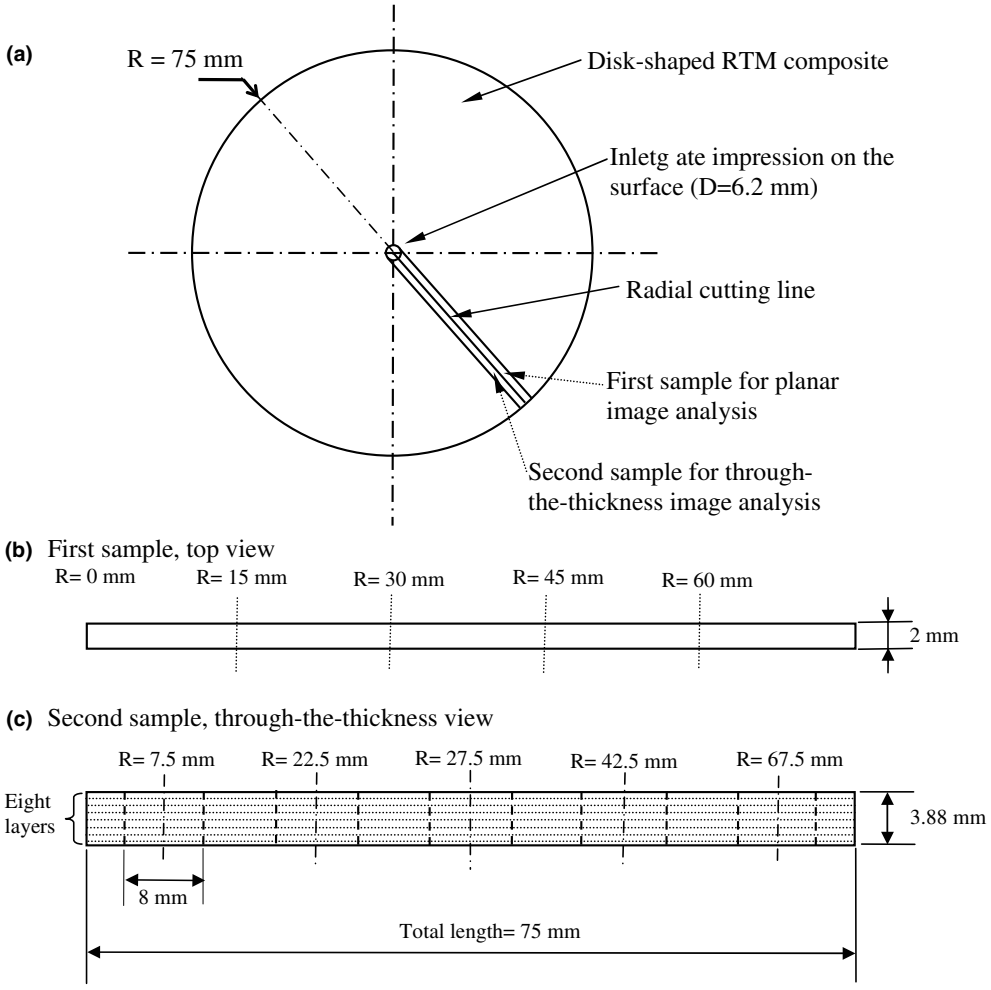

Fig. 1. Spatial arrangement of investigated samples: (a) location of samples within the composite disk, (b) first sample partitioned into five 15-mm-long radial regions for planar void analysis, (c) second sample partitioned into five 8-mm-radial regions and eight through-the-thickness layers.

located at different thickness locations of the sample are visually differentiated to permit void characterization through-the-thickness of the composite. A total of 960 captured frames, containing visually identified voids, are processed using the image analysis software Image Tool®. Image Tool® allows the manual measurement of void area and maximum length, thus eliminating the uncertainty usually introduced when utilizing threshold levels to automatically determine voids from microscopic images.

3. Results and discussion

3.1. Average void content

Most, if not all, void studies characterize void morphology two-dimensionally, which limits the understanding of void formation and mobility mechanisms in RTM composites. Post-cure studies investigating void size and shape often use microscopic image analysis only through-the-thickness of the composite [4–6,20,22,25,29–31,35,38]. While studies on void formation during mold filling determine void morphology and distribution via monitoring flow front progression from the planar view [1,10–13,17,18,26,33,34,36,39]. To the best of authors' knowledge, no study combines the two views to assess three-dimensional features of void morphology. As illustrated by the 50× magnification images shown in Fig. 2, fiber orientation distributions and fiber clustering for the planar and through-the-thickness views are fundamentally different: Fibers are seen as more homogeneously distributed through the composite thickness (Fig. 2(a) and (c)), while the planar view offers zones with very high fiber concentration (Fig. 2(b)), and large matrix-rich regions (Fig. 2(d)). The way successive preform layers are arranged inside the mold cavity prior to mold filling is a plausible cause for the observed difference in architecture between the two views of the same composite. Another conceivable source for these architectural discrepancies may be related to up to 77% variation in planar densities of the utilized reinforcement. Planar density of utilized preforms was found to vary between 0.3141 and 0.5564 kg/m^2, thus yielding significant variations of spatial fiber concentration. These values were calculated from more than five hundred circular performs cut from the same randomly-oriented fiber glass roll used in this study.

Void contents obtained for the eight through-the-thickness layers depicted in Fig. 1(c) are shown in Table 2. Void content is found to vary between 1.25% and 2.62% through-the-thickness. This non-uniformity can rise from uneven spaces between the four preform layers, or between the preform and the mold walls. It can also originate from the potential variations in the fluid front velocity across the thickness of the mold cavity. Thus, considerable differences in overall void content obtained from the two samples are also expected. After processing all the void data, planar and through-the-thickness average void contents of 2.56% and

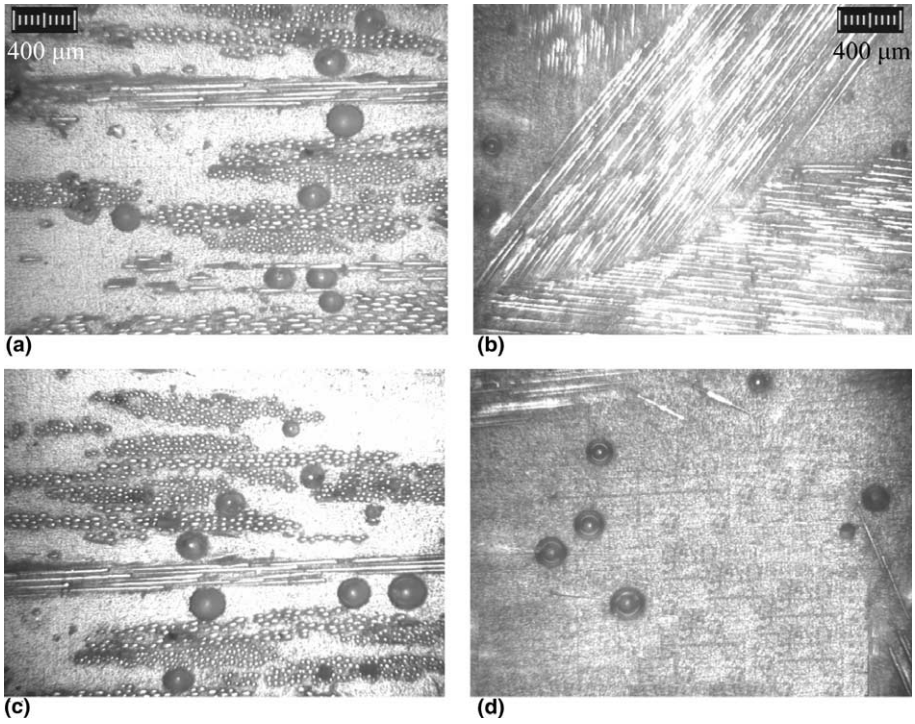

Fig. 2. Representative microscopic images obtained at 50× magnification from through-the-thickness (left column) and planar (right column) views.

2.15% are calculated, respectively. However, average void content obtained from the planar view can only be compared to void content in the same layer of the composite. Since a 0.67-mm-thick layer was machined from the top of the planar sample; the obtained planar void content of 2.56% should be compared to that of 2.58% obtained from the second layer (Table 2). The two values are very similar; suggesting that void contents obtained from planar views would depend primarily on the through-the-thickness location of the scanned plane, and thus may vastly vary from one layer to the other. On the other hand, void contents obtained from through-the-thickness view, when the entire composite thickness is examined for voids, are not prone to such variations [38]. Consequently, the void content determined from through-the-thickness view would be more representative of the actual void content in RTM composites.

3.2. Location of voids

Void proximity to fibers can be assessed differently from planar and through-the-thickness views. Voids seen in matrix-rich areas from the planar view can in fact be in contact with fibers in other layers below the polished surface. To study this morphological feature, we introduced a classification of voids based on their proximity to fibers and analyzed both planar and through-the-thickness sections. In addition, this classification can help estimate possible adverse effects of each void on mechanical properties. Voids located only in the matrix reduce the load bearing cross-section of the composite, while those located in contact with fibers are also detrimental to fiber/matrix adhesion. Three void locations are defined: First location is defined as areas rich in matrix and not comprising any fibers. Voids encountered in this location are totally surrounded by the epoxy matrix and are referred to as *matrix voids*. Second location is defined as areas rich in fibers, where the area is primarily composed of reinforcing preform. Voids in these locations are situated within fiber bundles (i.e., intra-tow voids) and are referred to as *preform voids*. Finally, transition location is defined as the remaining locations other than the other two defined above. Voids found in this location are referred to as *transition voids* and are always positioned adjacent to the preform but not inside fiber tows.

Fig. 3 depicts sample images obtained from the two views containing voids obtained from the three zones defined above at 200× magnification. Based on the categories defined earlier, voids seen in Fig. 3(a) are *preform voids* along with similar voids from Fig. 3(b)–(d). The voids seen adjacent to fiber tows in Fig. 3(e) and (f) are *transition voids*. Finally, the void depicted at the left side of Fig. 3(b) is considered a *matrix void*.

Fig. 4 shows the contributions of voids encountered within different locations to the average void content of the whole composite. From the planar view, voids seem to be concentrated in the matrix rich zone contributing 1.5% to the 2.56% overall void content. At the same time, intra-tow voids, located inside the preform, do not seem to constitute a significant portion of the voidage of the whole composite. Only 17.6% of the 2.15% overall voidage (i.e., 0.43%) is identified as *preform voids*. In contrast, through-the-thickness voidage shows a different distribution. While the *transition voids* showed the highest contribution at 1.31%, the *preform* and *matrix voids* contributed 0.72% and 0.15%, respectively. Thus, 94.4% of the total voidage is observed either inside or right next to the preform when through-the-thickness view is used.

Due to the difference in fiber orientation patterns between planar and through-the-thickness views described above, classification of void locations based on through-the-thickness view is believed to better characterize the actual locations of voids throughout the composite. For instance, many voids that are classified as *matrix voids* in the planar view might be in contact with fibers at composite layers above or below the observed plane, thus belonging in reality to *transition voids* category. As shown in Fig. 2(a) and (c), the stacking of preform layers does not leave adequate space between fiber tows to have a significant occurrence of *matrix voids*.

Utilizing the modified capillary number can help understand formation mechanisms of voids involved in the micro-scale flow during fluid front progression. Fig. 5 illustrates void contents measured by Rohatgi et al. [13] at different modified capillary number using model fluids. Void contents measured in the current study for the five radial regions from both views are also presented. Despite the difference in fiber content (i.e. 17.5% in the current study vs. 43% in Rohatgi et al.) and the fiber orientation (i.e. random-mats vs. unidirectional), the measured void contents seem to

Table 2
Variation in voidage through the composite disk thickness

	Layer 1	Layer 2	Layer 3	Layer 4	Layer 5	Layer 6	Layer 7	Layer 8
Thickness (mm)	0.5	0.5	0.5	0.5	0.5	0.5	0.5	0.38
Void content	2.30%	2.58%	1.52%	2.62%	2.47%	2.21%	2.61%	1.25%
Planar void density (void/mm^2)	10.78	11.51	9.25	11.51	10.84	10.67	12.12	6.37

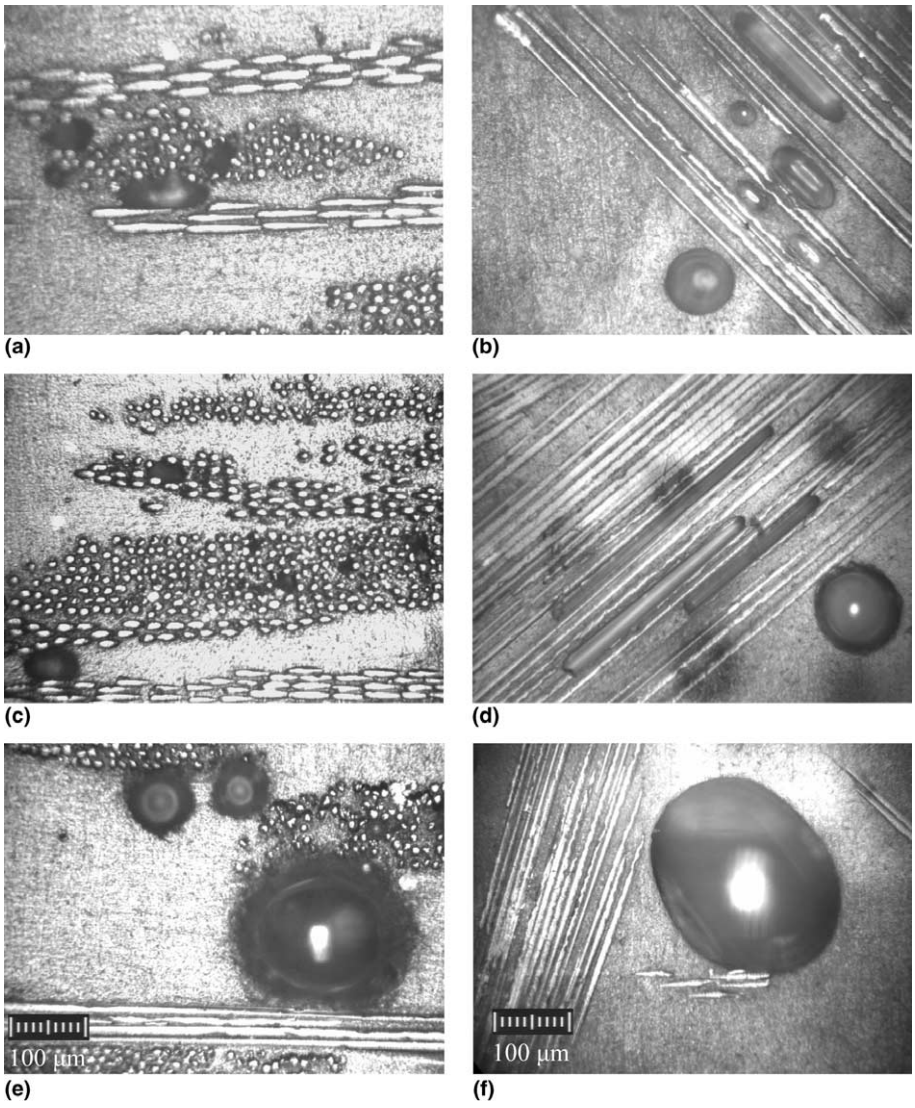

Fig. 3. Planar and through-the-thickness areal void density distributions for different void shapes.

fit well with those obtained from different model fluids. In addition, within the range of modified capillary number for the molded composite (see Table 1), Fig. 5 predicts voids to be primarily intra-tow microvoids. Incidentally, this prediction is corroborated by the through-the-thickness view where most voids are seen as intra-tow voids.

3.3. Variation of void size

Void size is reported to affect void mobility [22], such that larger voids have longer perimeters and thus yield larger adhesion forces. Small voids, on the other hand, have lower adhesion forces and therefore become more mobile. Consequently, identifying void size distribution can prove useful in the choice of void removal methods. To quantify void sizes, the surface area, A, of each captured void is measured using the image analysis software Image Tool®. An equivalent diameter, D_{eq}, is defined to classify void sizes as:

$$D_{eq} = \sqrt{\frac{4A}{\pi}}, \tag{2}$$

where A is the measured area of the void. Planar and through-the-thickness size distributions based on D_{eq} are represented in Fig. 6. Both are lognormal distributions with only one peak, unlike typical bi-modal void distributions in fiber reinforced composites that exhibit two peaks [18]. The first peak often represents intra-tow micro-voids while the second inter-tow macro-voids. As discussed previously, the calculated range of modified capillary numbers of 0.13–1.15 implies that the formed voids are primarily intra-tow, micro-voids [12,13], which explains why only few large macro-voids were encountered within the composite. Although the standard deviations of both distributions appear

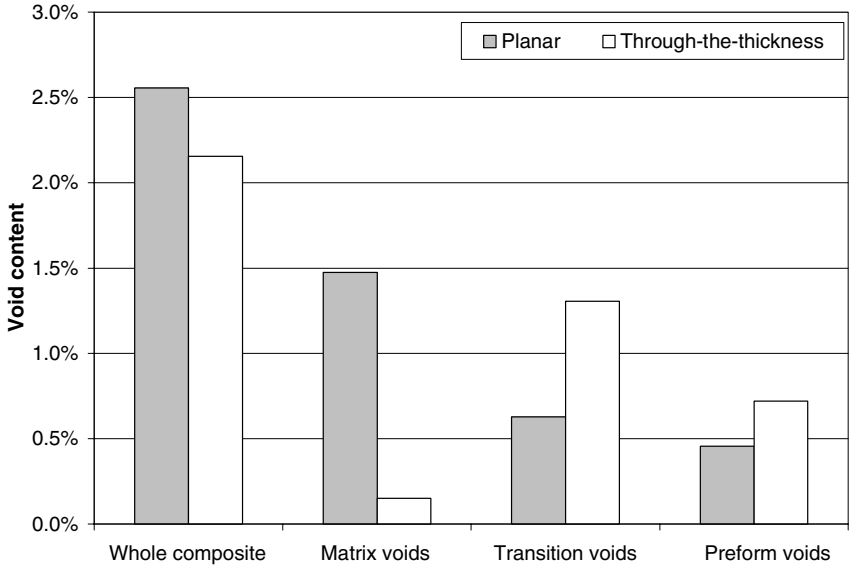

Fig. 4. Planar and through-the-thickness void content contributions of voids located at different locations of the composite.

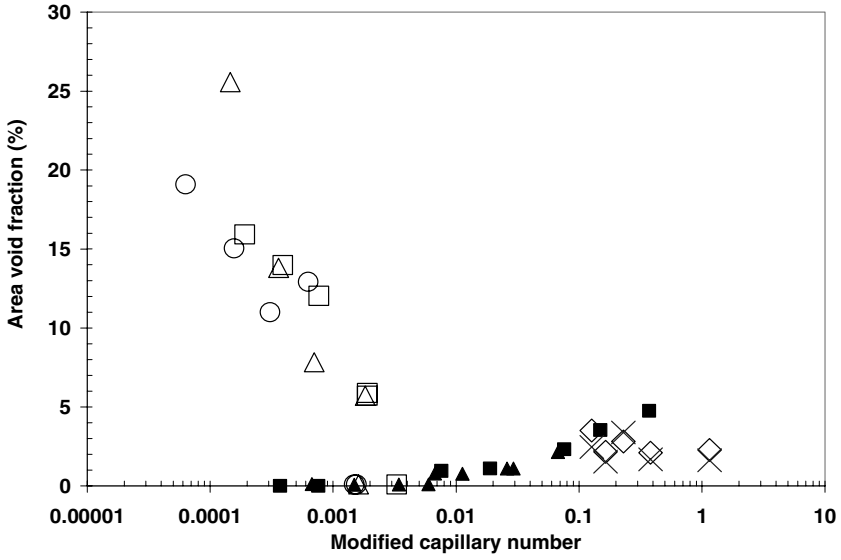

Fig. 5. Effect of modified capillary number on void formation. Data for model fluids taken from Rohatgi et al. [13]: (□) silicone oil, macro-voids; (■) silicone oil, micro-voids; (△) DOP oil, macro-voids; (▲) DOP oil, micro-voids; (○) ethylene glycol, macro-voids; (●) ethylene glycol, micro-voids; and from the current study obtained from the: (◇) Planar view; (X) Through-the-thickness view.

comparable, a slight "shift" of the distribution towards smaller voids is observed from the planar to the through-the-thickness view. The two size distributions present mean values of 59.33 μm for the through-the-thickness view and 66.65 μm for the planar view, but have very close standard deviations of 26.88 and 26.65 μm, respectively. This variation in the size distribution viewed from two planes is compensated by an opposite variation in areal void density. Through-the-thickness view showed a void density of 9.83 voids/mm^2, while the planar view showed only 6.33 voids/mm^2 in areal void density. In short, voids are seen in average slightly fewer but larger in the planar view. The observed difference in void size distribution when seen from the two views, especially the mean equivalent diameter, can be explained by the existence of long cigar-shaped intra-tow voids inside fiber bundles (Fig. 3(b) and (d)). The preform is mostly planar, thus these cigar-shaped voids are seen only as small intra-tow voids when observed from through-the-thickness view, but are seen in full in the planar view.

In order to categorize void sizes, three different size ranges are defined. Large voids are defined as those voids with an equivalent diameter greater than 100 μm, i.e. $D_{eq} > 100$ μm; while voids with an equivalent diameter lower than 50 μm are regarded as small

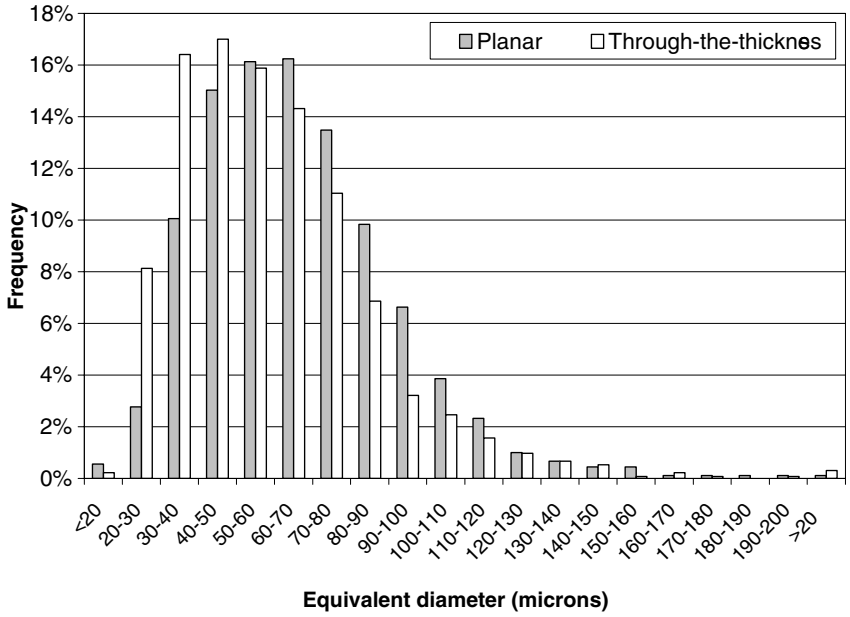

Fig. 6. Planar and through-the-thickness size distributions based on equivalent diameter.

voids. Intermediate equivalent diameter values, i.e. $50\ \mu m < D_{eq} \leqslant 100\ \mu m$, correspond to medium size voids. Using these categories, concise planar and through-the-thickness void size distributions are obtained as shown in Fig. 7. Void size distributions for the whole composite and for the *preform voids* are presented for both samples. Fig. 7 indicates that small voids encountered within the preform rise from a 40.21% of the total voids for the planar view to more than 66% for through-the-thickness view. This steep increase in relative percentage of small voids found within the preform combined with almost no change in *matrix* and *transition voids* size distributions confirms that only *preform voids* cause the change in average void size between the two views, leading to the 13% increase in average void size observed in Fig. 6. Based on these findings, the actual void size distribution seems to be revealed better by the planar view as some of the larger voids are not fully seen in through-the-thickness-view.

3.4. Variation in void shape

As Figs. 2 and 3 illustrate, considerably different void shapes are encountered in the two orthogonal views of

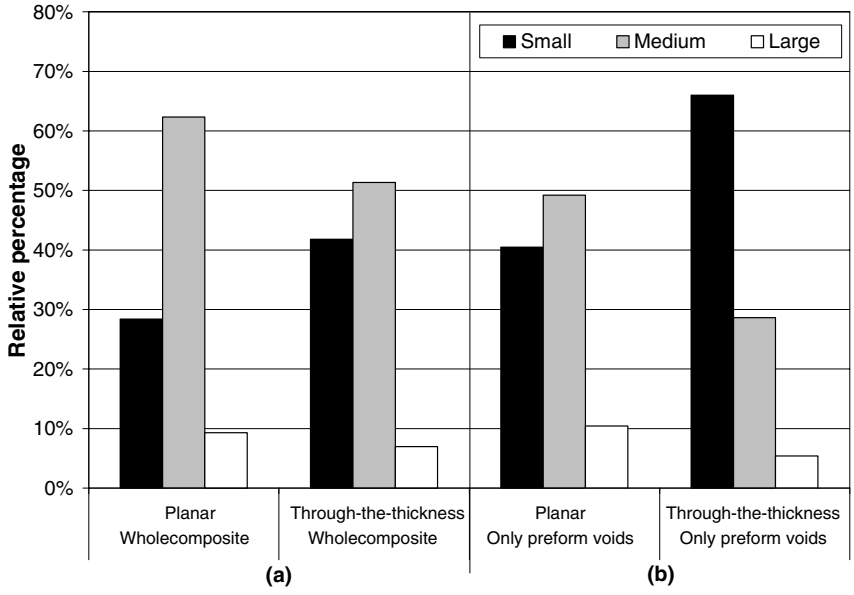

Fig. 7. Size distribution of voids obtained from planar and through-the-thickness views when: (a) considering the whole composite; (b) considering only *preform voids*.

the composite. In order to quantify these differences in void shapes, both geometrical and quantitative void characteristics are combined. First, based on the observed shape, voids are divided into three groups: Irregular, cylindrical, and spherical voids. Irregular voids are defined as those presenting a non-convex planar surface area, that is, one can find two different points within the void that can be connected by a straight line that intersects the void boundary. Additionally, cylindrical voids are defined as cigar-shaped voids, observed almost exclusively inside fiber tows when seen from the planar view (Fig. 3(b) and (d)). Excluding those two categories, remaining voids are mostly spherical (Fig. 3(e) and (f)), although some of them do not present a perfect circular symmetry (Fig. 3(f)).

To classify this variation in voids' roundness, a quantitative measure of geometrical circularity of voids is used. The data obtained from captured voids is further processed by introducing the shape ratio, R_s, defined for each void as the equivalent diameter obtained from Eq. (2) divided by the measured maximum length, L_{max}, within a void:

$$R_s = \frac{D_{eq}}{L_{max}}. \quad (3)$$

Using this shape ratio, spherical voids are divided into two categories: circular voids, and elliptical voids. Since an ideal circle is represented by $R_s = 1$, only voids with shape ratios above 0.95 ($0.95 < R_s \leqslant 1$) are considered circular voids (bottom of Fig. 3(b)). Voids with shape ratios lower than 0.95 comprise a minor axis that could be significantly smaller than the maximum length. Thus, the circular symmetry is lost, the voids appear as ellipses, and are defined as elliptical voids. Typical examples of small irregular voids are presented in Fig. 3(a) and (c), with equivalent diameters raging between 17.23 and 49.65 μm. Similar intra-tow voids are seen as cylindrical voids in the planar view as shown in Fig. 3(b) and (d). A large circular void is seen at the bottom of Fig. 3(b) ($D_{eq} = 85.37$ μm and $R_s = 0.99$). Finally, Fig. 3(f) exemplifies a large elliptical void exhibiting an equivalent diameter of 250.25 μm and a shape ratio of 0.91.

As voids with different shapes are known to affect the mechanical performance of the composite differently [6,40], the number of voids having a detrimental shape is more important than their contribution to the void content obtained for the whole composite. Therefore, areal void density is used here to present planar and through-the-thickness shape distributions. The resulting shape-voidage distribution is presented in Fig. 8.

Areal void densities obtained from the two samples are considerably different. The areal void density of 6.33 voids/mm^2 in the planar view is only 64.4% of the through-the-thickness areal void density of 9.83 voids/mm^2. As shown in Fig. 8, cylindrical voids are not observed through the composite thickness. Since the sample used for through-the-thickness analysis is cut at an angle to most fiber bundles – potential beds for cylindrical voids – all cylindrical voids are truncated at an angle with respect to their longitudinal axis, and are seen as either small irregular, or small elliptical voids. This can explain the considerable increase in areal void density of elliptical voids from 0.48 voids/mm^2 in the planar view to 2.91 voids/mm^2 in the through-the-thickness view. In addition, irregular areal void density jumps from 0.25 voids/mm^2 in the planar view to 3.48 voids/mm^2 in through-the-thickness view. This increase can also be explained, in addition to the presence of cylindrical voids, by the difference in fiber placement and orien-

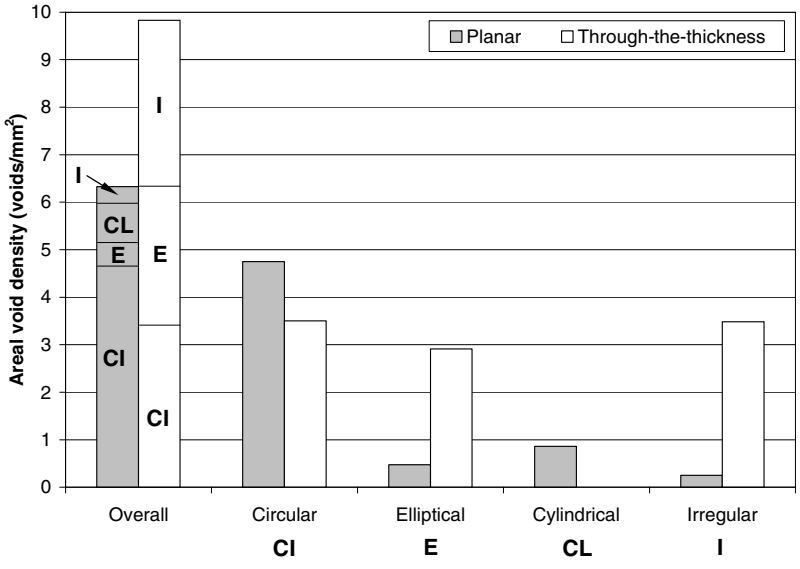

Fig. 8. Planar and through-the-thickness areal void density distributions for different void shapes.

tation patterns for the two views illustrated in Fig. 2. As argued earlier, many voids that are seen in the matrix in a particular planar view are in reality in contact with fiber tows at composite layers above or below the observed plane. Therefore, even if the planar view of a void is circular, the void may in fact present an irregularity where it comes in contact with fiber bundles, and is seen as an irregular void through-the-thickness. This latter fact can also explains the drop in circular areal void density from 4.75 in planar view to 3.50 voids/mm^2 in through-the-thickness view. These findings imply that neither planar nor through-the-thickness views can fully represent the actual void shape distribution. A combination of the two must be incorporated in order to fully assess the three-dimensional shape morphology of the voids.

3.5. Voidage variation along the radius of the molded disk

When resin injection is performed at a constant volume flow rate through a constant mold cross-section, the fluid front velocity, and subsequently the capillary number, do not depend on the distance from the injection inlet. Consequently, the voidage along the composite part may not vary much with respect to the inlet distance. In contrast, the impregnation in the current case is carried out at constant volume flow rate for a center-gated disk-shaped cavity. Hence, the fluid front velocity and the modified capillary number change as the flow progresses. This change in capillary number is likely to yield a radially non-uniform void distribution.

To determine the effect of radial distance on voidage and void morphology, five equivalent radial regions were defined, as shown in Fig. 1, for both studied samples. Fig. 9 shows planar and through-the-thickness void content distributions along the direction of the flow during mold filling. Each radial region is referred to using the radial distance from the injection gate to its center as shown in Table 1. As shown in Fig. 5, void content is expected to increase moderately with increasing modified capillary number [12,13]. Accordingly, void content is predicted to decrease with increasing radial distance from the injection gate. Moreover, at longer distances from the injection gate (i.e., lower capillary number), slower moving fluid front is expected to trap smaller, more circular, and fewer voids [30]. Nevertheless, both planar and through-the-thickness void content radial distributions, given in Fig. 9, do not clearly show this trend.

To understand the mechanisms behind this radial distribution, void contents from different void locations (i.e., *matrix*, *transition*, and *preform voids*) are segregated. Since through-the-thickness view is believed to better represent the actual location distribution of voids, only through-the-thickness results are utilized here. Fig. 10 shows radial distribution of *matrix*, *transition*, and *preform voids* taken from through-the-thickness view. Although radial distance does not seem to have an effect on the distribution of*matrix voids*, clear trends are observed for the relative content of *transition* and *preform voids*. The relative contribution of *preform voids* to the overall void content decreases from 47.23% in the third region to 14.55% in the fifth region. In contrast, contribution of *transition voids* increases from 37.50% in the third region to 77.40% in the fifth region.

Reduction in *preform void* content along the flow direction is in concordance with the predicted void behavior based on capillary number analysis discussed earlier. On the other hand, higher pressure inside the mold would force the voids the shrink or even dissolve

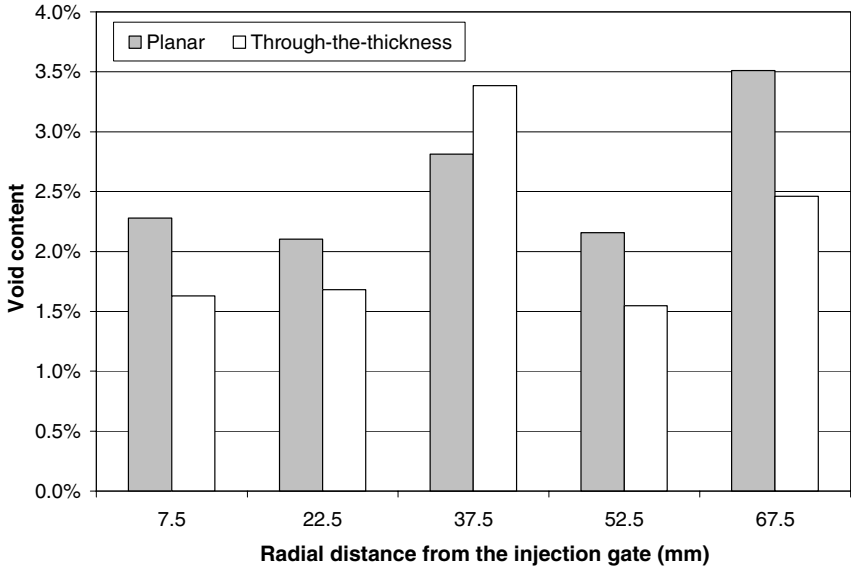

Fig. 9. Planar and through-the-thickness radial distributions of void content.

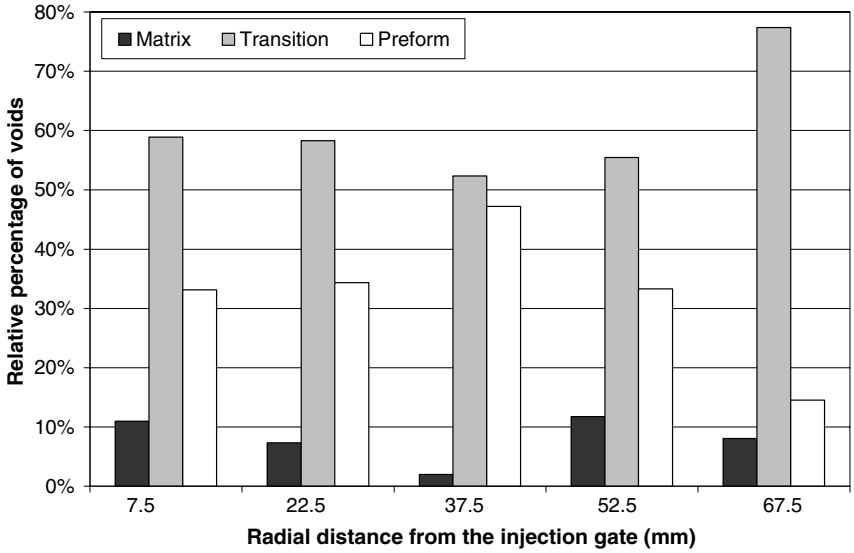

Fig. 10. Through-the-thickness radial voidage distribution for different void locations in the composite.

into the resin [36,37]. Therefore, void sizes during mold filling – where pressure levels reach 500–600 kPa – and after the pressure inside the mold cavity dropped to atmospheric levels at the end of mold filling would be different. Hence, voids would have been much smaller during mold filling and expand to larger sizes as the pressure drops after filling is complete. Unlike *preform voids* that are trapped inside fiber tows, *transition* and *matrix voids* are relatively free to move during mold filling, particularly if they are sufficiently small [22,23]. Consequently, there is an elevated probability of their transport towards the exit vents. Moreover, closer to the injection gate, voids experience flow and are subject to shear deformation as well as increasing pressure longer. Therefore, although *matrix* and *transition voids* may have formed as predicted by the capillary number analysis (Fig. 5), their radial distribution might have been rearranged during mold filling.

To better understand this phenomenon, a closer look at the radial distribution of *preform voids* can be of great assistance. Fig. 11 illustrates planar size distribution of *preform voids* in the radial direction. Planar view is used here since cylindrical voids with very different sizes would appear the same when sectioned by through-the-thickness view, hence giving a misleading representation of the investigated morphological feature. The faster moving fluid front in the first radial region, led by viscous flow, is expected to trap larger *preform voids*. As the radial distance from the injection gate increases, slower fluid fronts are anticipated to

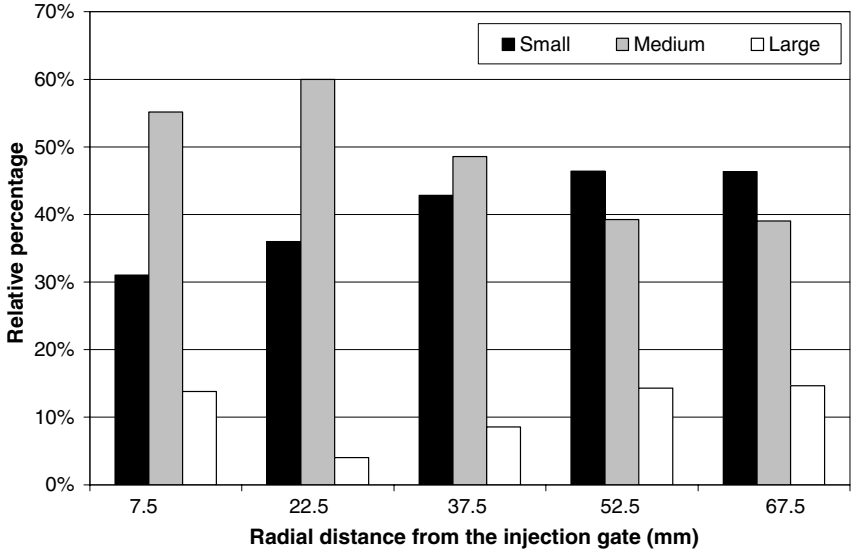

Fig. 11. Planar *preform void* size distribution along the flow direction.

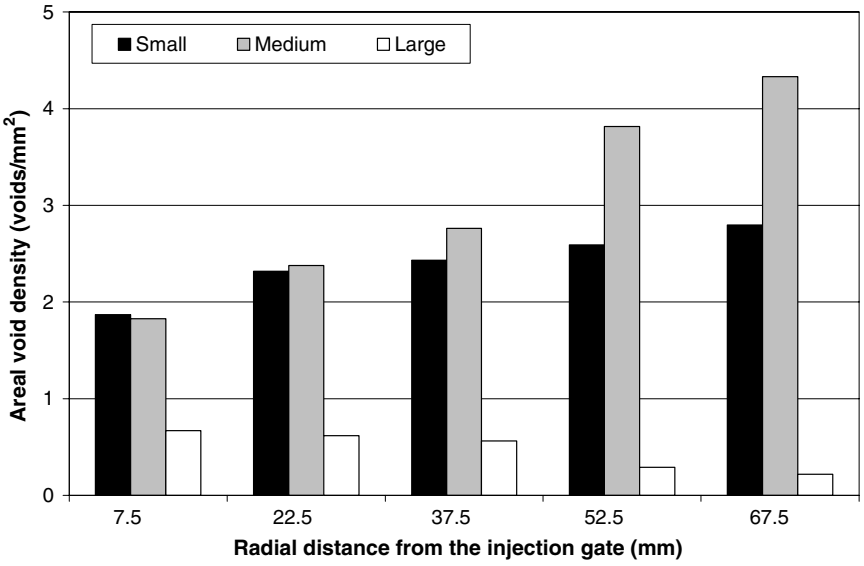

Fig. 12. Areal density of different-sized mobile voids (i.e., combined matrix and transition) along the flow direction based on through-the-thickness view.

capture fewer and smaller *preform voids*, yielding lower void contents at higher radial distances from the injection gate. In Fig. 11, a gradual shift towards smaller trapped intra-tow voids is observed as the relative percentage of small *preform voids* increases – almost linearly – from 31.03% to 46.34% between the first and fifth radial regions, registering almost 50% increase. In contrast, medium *preform void* relative percentage sees a 34.97% decrease between the second and fifth radial regions (i.e., 60% to 39.02%). In addition, the average preform *void* size decreases from 68.56 μm in the first radial region to 61.20 μm in the fifth. These definite trends prove that voids – at least at the formation stage – correlate well with the predictions based on the capillary number analysis. However, once voids are formed at a radial location, they are subjected to increasing pressures and shear stresses during filling, making them prone to become smaller and move radially away from the inlet. *Preform voids* cannot move since they are trapped inside fiber bundles. Hence, only *matrix* and *transition voids* are potential mobile voids. Radial size distributions of *matrix* and *transition* voids are investigated to characterize the behavior of mobile voids in the flow direction. Combined radial matrix and transition areal void densities are depicted in Fig. 12.

Large voids are less likely to move during resin injection since they have higher adhesion force caused by their longer perimeters [22,23]. The areal density of large mobile voids is observed to decrease steadily with increasing distance from the injection gate, from 0.67 to 0.22 voids/mm^2 between the first and fifth radial regions. This trend is an additional confirmation of the effect of capillary number on void formation since large voids tend to resist transport and stay where they were initially formed. In contrast, medium and small mobile voids respective contributions augment away from the inlet. Both small and medium mobile areal void densities increase both steadily along the flow from 1.87 and 1.83 voids/mm^2 at 7.5 mm from the injection gate, respectively, to 2.80 and 4.33 voids/mm^2 at 67.5 mm from the injection gate. However, the contribution of medium mobile voids shows a higher increase of almost 140%, while small mobile voids showed a more modest 50% increase between the first and fifth radial regions. Therefore, spatial distributions of mobile voids with an equivalent diameter smaller than 100 μm are essentially dictated by their mobility in a molded composite. Thus, voids formed in the earlier radial regions at higher *Ca** can be transported towards the exit, yielding slightly lower void content then expected as seen in Fig. 5. In summary, most voids observed in RTM composites are formed based on the local capillary number, and a large number of potential mobile voids (i.e., matrix and *transition voids*) are then transported during mold filling leading to a complex spatial distribution.

4. Conclusions

Three-dimensional features of void morphology in resin transfer molded composites are investigated. Voids are assessed via microscopic image analysis from both planar and through-the-thickness surfaces of a disk-shaped, E-glass/epoxy composite with a fiber content of 17.5%. A 2.15% void content is obtained from the through-the-thickness surface and is believed to be representative of the actual void content in the studied part. The planar void content of 2.56%, on the other hand, compares well with the 2.58% void content ob-

tained from the corresponding through-the-thickness layer. The two investigated surfaces also revealed differences in void morphology. Relatively large cylindrical voids, observed in cigar shapes in the planar surface, appear only as small irregular or elliptical voids on through-the-thickness surface. These observed differences in void morphology led to a 13% decrease in the average void size from planar to through-the-thickness views. Moreover, in the planar view, 57.4% of the voidage is observed to be surrounded completely by the matrix; whereas 94.4% of the total voidage in through-the-thickness surface is found to be either inside or right next to fiber tows. Along the flow direction, combined effects of void formation by mechanical entrapment and void mobility formed a complex radial void distribution. 33% fewer inter-tow voids are observed to be trapped mechanically near the exit compared to the inlet region. Most of the medium and small mobile voids (i.e., *matrix and transition voids*) seem to migrate towards the exit during resin injection, thus yielding a 93% increase of such voids near the exit. These findings are believed to be applicable not only to RTM, but generally to other composites manufactured by liquid molding processes with nonuniform flow kinematics.

References

[1] Abraham D, Matthews S, Mcllhagger R. A comparison of physical properties of glass fiber epoxy composites produced by wet lay-up with autoclave consolidation and resin transfer moulding. Comp Part A 1998;29:795–801.

[2] Shojaei A, Ghaffarian SR, Karimian SMH. Modeling and simulation approaches in the resin transfer molding process: a review. Polym Comp 2003;24(4):96–109.

[3] Judd NCW, Wright WW. Voids and their effects on the mechanical properties of composites – an appraisal. SAMPE J 1978;14(1):10–4.

[4] Ghiorse SR. Effect of void content on the mechanical properties of carbon/epoxy laminates. SAMPE Qtly 1993;Jan:54–9.

[5] Olivero KA, Barraza HJ, O'Rear EA, Altan MC. Effect of injection rate and post-fill cure pressure on resin transfer molded disks. J Comp Mater 2002;36(16):2011–28.

[6] Goodwin AA, Howe CA, Paton RJ. The role of voids in reducing the interlaminar shear strength in RTM laminates. In: Scott ML, editor. Proceedings of ICCm-11, vol. IV. Australian Composite Structures Society; 1997. p. 11–9.

[7] Harper BD, Staab GH, Chen RS. A note on the effect of voids upon the hygral and mechanical properties of AS4/3502 graphite/epoxy. J Comp Mater 1987;21:280–9.

[8] Hoppel C, Bogetti T, Newill JF. Effects of voids on moisture diffusion in composite materials. In: Proceedings of the American Society for Composites 2000;1094–1102.

[9] Stabler WR, Tatterson GB, Sadler RL, El-Shiekh AHM. Void minimization in the manufacture of carbon fiber composites by resin transfer molding. SAMPE Qtly 1992;Jan:38–42.

[10] Patel N, Lee LJ. Effect of fiber mat architecture on void formation and removal in liquid composite molding. Polym Comp 1995;16(5):386–99.

[11] Mahale AD, Prud'Homme RK, Rebenfeld L. Quantitative measurement of voids formed during liquid impregnation of nonwoven multifilament glass networks using an optical visualization technique. Polym Engr Sci 1992;32(5):319–26.

[12] Patel N, Rohatgi V, Lee JL. Micro scale flow behavior and void formation mechanism during impregnation through a unidirectional stitched fiberglass. Mater Polym Engr Sci 1995;35(10):837–51.

[13] Rohatgi V, Patel N, Lee JL. Experimental investigation of flow induced microvoids during impregnation of unidirectional stitched fiberglass mat. Polym Comp 1996;17(2):161–70.

[14] Chan AW, Morgan RJ. Modeling preform impregnation and void formation in resin transfer molding of unidirectional composites. SAMPE Qtly 1992;Apr:48–52.

[15] Chui WK, Glimm J, Tangerman FM, Jardine AP, Madsen JS, Donnellan TM, et al. Porosity migration in RTM. In: Proceedings of the Ninth International Conference of Numerical Methods in Thermal Problems 1995:1323–34.

[16] Lundström TS. Measurement of void collapse during resin transfer moulding. Comp Part A 1997;28:201–14.

[17] Patel N, Lee JL. Modeling of void formation and removal in liquid composite molding. Part I: Wettability analysis. Polym Comp 1996;17(1):96–103.

[18] Patel N, Lee JL. Modeling of void formation and removal in liquid composite molding. Part II: Model development and implementation. Polym Comp 1996;17(1):104–14.

[19] Binetruy C, Hilaire B, Pabiot J. Tow impregnation model and void formation mechanisms during RTM. J Comp Mater 1998;32(3):223–45.

[20] Kang MK, Lee WI, Hahn HT. Formation of microvoids during resin-transfer molding process. Comp Sci Technol 2000;60:2427–34.

[21] Lundström TS. Bubble transport through constricted capillary tubes with application to resin transfer molding. Polym Comp 1996;17(6):770–9.

[22] Shih C-H, Lee LJ. Analysis of void removal in liquid composite molding using microflow models. Polym Comp 2002;23(1):120–31.

[23] Blackmore B, Li D, Gao J. Detachment of bubbles in slit microchannels by shearing flow. J Coll Interf Sci 2001;241(2):514–20.

[24] Lundström TS, Gebart BR. Influence from process parameters on void formation in resin transfer molding. Polym Comp 1994;15(1):25–33.

[25] Shih C-H. Liquid composite molding of tackified fiber reinforcement: preforming and void removal. PhD Thesis, Ohio State University, Department of Chemical Engineering, 2000.

[26] Abraham D, Mcllhagger R. Investigation into various methods of liquid injection to achieve mouldings with minimum void content and full wet out. Comp Part A 1998;29:533–9.

[27] Ikegawa N, Hamada H, Maekawa Z. Effect of compression process on void behavior in structural resin transfer molding. Polym Engr Sci 1996;36(7):953–62.

[28] Choi JH, Dahran CKH. Mold fill time and void reduction in resin transfer molding achieved by articulated tooling. J Comp Mater 2002;36(19):2267–85.

[29] Barraza HJ, Hamidi YK, Aktas L, O'Rear EA, Altan MC. Porosity reduction in the high-speed processing of glass fiber composites by resin transfer molding (RTM). J Comp Mater 2003;38(3):195–226.

[30] Hamidi YK, Altan MC. Spatial variation of void morphology in resin transfer molded e-glass/epoxy composites. J Mater Sci Lett 2003;22(24):1813–6.

[31] Hamidi YK, Aktas L, Altan MC. Formation of microscopic voids in resin transfer molded composites. J Engr Mater Tech 2004;126(4):420–6.

[32] Blake JW. Studies in reaction injection mold filling. PhD Thesis, University of Minnesota, Department of Chemical Engineering and Material Science, 1987.

[33] Patel N. Micro scale flow behavior, fiber wetting and void formation in liquid composite molding. PhD Thesis, Ohio State University, Department of Chemical Engineering, 1994.
[34] Rohatgi V. Liquid molding of textile reinforcements: analysis of flow induced voids and effects of powder coating on preforming and moldability. PhD Thesis, Ohio State University, Department of Chemical Engineering, 1995.
[35] Ghiorse SR. A Comparison of void measurement methods for carbon/epoxy composites. U.S. Army Materials Technology Laboratory 1991; Report MTL-TR: 91–13.
[36] Chen Y-T, Davis HT, Macosko CW. Wetting of fiber mats for composites manufacturing: I. Visualization experiments. AICHE J 1995;41(10):2261–73.
[37] Roychowdhury S. Void formation and growth in amorphous thermoplastic polymeric materials. PhD Thesis, University of Delaware, Department of Material Science and Engineering, 1995.
[38] Santulli C, Garcia Gil R, Long AC, Clifford MJ. Void content measurement in commingled E-glass/polypropylene composites using image analysis from optical micrographs. Sci Engr Comp Mater 2002;10(2):77–90.
[39] Han K, Lee LJ. Dry spot formation and changes in liquid composites molding: II. Modeling and simulation. J Comp Mater 1996;30(13):1458–74.
[40] Wisnom MR, Reynolds T, Gwilliam N. Reduction in interlaminar shear strength by discrete and distributed voids. Comp Sci Technol 1996;56(1):93–101.